Hyperfine Interact (2017) 238:68
https://doi.org/10.1007/s10751-017-1440-8

What the multiline signal (MLS) simulation data with average of weighted computations reveal about the Mn hyperfine interactions and oxidation states of the manganese cluster in OEC?

Bernard Baituti[1]

Abstract Understanding the structure of oxygen evolving complex (OEC) fully still remains a challenge. Lately computational chemistry with the data from more detailed X-ray diffraction (XRD) OEC structure, has been used extensively in exploring the mechanisms of water oxidation in the OEC (Gatt et al., J. Photochem. Photobiol. B **104**(1–2), 80–93 2011). Knowledge of the oxidation states is very crucial for understanding the core principles of catalysis by photosystem II (PSII) and catalytic mechanism of OEC. The present study involves simulation studies of the X-band continuous wave electron-magnetic resonance (CW-EPR) generated S_2 state signals, to investigate whether the data is in agreement with the four manganese ions in the OEC, being organised as a '3+1' (trimer plus one) model (Gatt et al., Angew. Chem. Int. Ed. **51**, 12025–12028 2012; Petrie et al., Chem. A Eur. J. **21**, 6780–6792 2015; Terrett et al., Chem. Commun. (Camb.) **50**, 8–11 2014) or 'dimer of dimers' model (Terrett et al. 2016). The question that still remains is how much does each Mn ion contribute to the "g2multiline" signal through its hyperfine interactions in OEC also to differentiate between the 'high oxidation state (HOS)' and 'low oxidation state (LOS)' paradigms? This is revealed in part by the structure of multiline (ML) signal studied in this project. Two possibilities have been proposed for the redox levels of the Mn ions within the catalytic cluster, the so called 'HOS' and 'LOS' paradigms (Gatt et al., J. Photochem. Photobiol. B **104**(1–2), 80–93 2011). The method of data analysis involves numerical simulations of the experimental spectra on relevant models of the OEC cluster. The simulations of the X-band CW-EPR multiline spectra, revealed three manganese ions having hyperfine couplings with large anisotropy. These are most likely Mn^{III} centres and these clearly support the 'LOS' OEC paradigm model, with a mean oxidation of 3.25 in

This article is part of the Topical Collection on *Proceedings of the 3rd Mediterranean Conference on the Applications of the Mössbauer Effect (MECAME 2017), Jerusalem, Israel, 5-7 June 2017*
Edited by Mira Ristic, Stjepko Krehula, Israel Nowik and Israel Felner

✉ Bernard Baituti
baitutib@biust.ac.bw

[1] Botswana International University of Science and Technology, Private Bag 16, Palapye, Botswana

Published online: 05 October 2017

the S_2 state. This is consistent with the earlier data by Jin et al. (Phys. Chem. Chem. Phys. (PCCP) **16**(17), 7799–812 2014), but the present results clearly indicate that heterogeneity in hyperfine couplings exist in samples as typically prepared.

Keywords High oxidation state (HOS) · Low oxidation state (LOS) · Continuous wave electron-paramagnetic resonance (CW-EPR) · Multiline (ML) signal · Photosystem II · Hyperfine couplings · Simulations

1 Introduction

Photosynthesis is divided into the light dependent reactions and the light independent reactions. The light dependent reactions have two main functional subunits known as Photosystem I and II. PSII contains the OEC, which utilises the interaction of four manganese ions and calcium ion (Mn_4/Ca catalytic cluster) for its function. PSII is a large enzyme protein complex found in the thylakoid membranes of oxygenic phototrophs, comprising algae, cyanobacteria as well as higher green plants. PSII (specifically the OEC) catalyses the oxidation of water into molecular oxygen, electrons and protons. It is located in the thylakoid membranes of chloroplasts. The chloroplast is an organelle and also one of the plastids present in advanced eukaryotic photosynthetic cells.

The OEC of PSII, located near the photo-oxidisable reaction centre P_{680}, contains a redox accumulating Mn_4/Ca catalytic cluster which binds water and passes electrons to the highly oxidising P^+_{680} centre via a redox active tyrosine residue (Tyr_Z). P_{680} is a special form of chlorophyll *a*, which is a primary electron donor of the photosystem II. P^+_{680} extracts electrons/protons from the two molecules of water (bound to Mn_4/Ca catalytic site) at physiological pH, and an overall oxidising potential of almost 1V versus standard hydrogen electrode. P^+_{680} is a highly oxidising radical generated when light induced primary charge separation occurs with the potential to oxidise water molecules, which is thermodynamically demanding and complex. The redox active tyrosine residue (Tyr_Z) located in the D1 polypeptide transfers an electron to the reaction centre (P^+_{680}) of PSII, from the OEC.

The OEC proceeds via five redox intermediate states known as 'S' states, categorised into four meta-stable states (S_0, S_1, S_2 and S_3) and one transient state (S_4). The subscripts in the 'S' states correspond to the stored oxidising equivalents [18]. The S_1 state is normally called the dark stable state of the OEC, and at low temperatures the Mn cluster becomes diamagnetic for dark-adapted samples [19]. The individual Mn oxidation states as well as average metal cluster oxidation level of the S_1 state are not yet resolved [1, 5, 20].

Umena et al. recently revealed the atomic level detail of the S_1 state of the Mn_4Ca at 1.9 Å resolution for the PSII structure [21], also at 2.1 Å resolution for the Sr/Ca-substituted enzyme [22] recently 1.95 Å resolution of the PSII structure [23]. The 2.1 Å, 1.95 Å and 1.9 Å resolution structures should be regarded as nominally S_1 (see Terrett et al., 2016). Two possibilities have been proposed for the redox levels of the Mn ions within the catalytic cluster, the so called 'HOS' and 'LOS' paradigms [1].

Jaszewski et al. have shown that the 'LOS' model, when metal ligand environmental effects are accounted for, is more consistent with the Mn K edge analysis. This computational study employed the latest Time Dependent DFT (TDDFT) methods [24]. The 'HOS' model is preferred based on empirical interpretation of Mn X-ray absorption spectroscopies applied to S_1 state of PSII and generation of S states by single flash turnover [25]. The S_1

state has an even net spin (integer-spin ground state), and the proposed oxidation arrangement of Mn ions in the cluster is $Mn^{III}Mn^{IV}Mn^{III}Mn^{II}$ (2.9 Å crystal structure form) or $Mn^{III}Mn^{III}Mn^{III}Mn^{III}$ (1.9 Å crystal structure form), using the 'LOS' paradigm, proposed at The Australian National University (ANU), with a mean cluster oxidation state of +3.0 [4]. Meanwhile using the 'HOS' paradigm arrangement of Mn ions in the cluster, it is proposed to be $Mn^{III}Mn^{III}Mn^{IV}Mn^{IV}$ [26], with mean cluster oxidation state of +3.5. The S_1 state may effectively contain lower order magnetic units: either a trinuclear cluster with a noninteracting monomer; or dinuclear cluster with a pair of noninteracting monomers, or a pair of non (or weakly) interacting dinuclear clusters or four noninteracting monomers [27]. Therefore in order to understand the structure of the OEC, characterisation of magnetic properties of the S_1 state is important.

The S_2 state has an odd number of electrons, and produces two basic EPR signal types due to the Mn cluster in OEC, which are influenced by the solvents, and cryoprotectant added to the PSII samples. The S_2 state has readily visible ML and $g4.1$ EPR signals and hence it has been the most studied of all the Kok cycle intermediates [28], due to the ease of experimental preparation and stability. The hyperfine structured spin ½ML signal is the most studied. In particular, the ML signal, is quantitatively explained, as arising mostly from magnetic contributions of a single Mn pair, in the III-IV oxidation state (anti-ferromagnetically coupled, net spin ½) within the OEC cluster. This pair is almost certainly Mn1-Mn2 [2]. The other pair, Mn3-4 (net spin 0), is then likely a III-III pair ('LOS' paradigm) or IV-IV pair ('HOS' paradigm), also anti-ferromagnetically coupled and near 'silent'. Its contribution to the ML signal state is small, but detectable [7]. Recent ENDOR studies at very low temperatures (∼2.5 K) favour large nuclear hyperfine contributions from Mn1 and Mn2, while the Mn3 and Mn4 contributions are small <100 MHz. Nuclear relaxation effects inhibit its observation in 'narrow' form samples [2].

It is presumed a single Mn centre oxidation occurs on $S_1 \rightarrow S_2$ state transition, with less structural change as shown by Mn extended X-ray absorption fine structure (EXAFS) results [29–32]. The shortening of the Mn-Mn interaction around 2.7 Å in $S_1 \rightarrow S_2$ state transition is observed, which likely results from oxidation state change of one Mn ($Mn^{III} \rightarrow Mn^{IV}$) as shown by EXAFS results [33]. In the 'LOS' paradigm this oxidation is believed to occur in the 'dangler' Mn4 in the cluster ($Mn^{II} \rightarrow Mn^{III}$), based on the 2.9 Å resolution crystal structure or $Mn^{III} \rightarrow Mn^{IV}$ (on Mn2) assuming the 1.9 Å resolution crystal structure [4]. A majority of PSII researchers still prefer the 'HOS' picture, mainly from spectroscopic interpretation, especially EPR and XANES-X-ray absorption near-edge structure [26, 34–38].

Structurally, the OEC is close to containing a pair of di-μ-oxo bridged Mn dimers, as there are two Mn-Mn EXAFS derived distances of ∼2.7 Å, which are long known [32, 39]. These are now known to be Mn1-2 and Mn2-3. Most likely, the Mn1-2 ions (Mn^{III}-Mn^{IV}) in the cluster are anti-ferromagnetically coupled, hence yielding a net spin of ½, while the other pair is presumed to be Mn^{III}-Mn^{III} (assuming the 'LOS' paradigm) or Mn^{IV}-Mn^{IV} (assuming the 'HOS' paradigm), and this pair yields a net spin zero. The two pairs are believed to weakly interact [40]. But lately this 'dimer of dimers' model has been disputed and the '3+1' or 'dangler' model has been frequently proposed [41].

The ML signals are the hyperfine structured ^{55}Mn hyperfine EPR signals, from net spin ½ground states, generated by trapping photosystem II (PSII) samples in the S_2 or S intermediates at cryogenic temperature [3]. The S_2ML signal exhibits approximately 20 resolved hyperfine peaks, with little g anisotropy, and the hyperfine interactions are readily measured in X-band CW-EPR due to them being large (couplings are of order 250 MHz or more).

The intrinsic hyperfine tensors of Mn^{III} and Mn^{II}/Mn^{IV} are distinctive, when all ions are high spin, with Mn^{III} being highly anisotropic as a Jahn-Teller d^4 ion, while Mn^{II}/Mn^{IV} are closer to isotropic (closed d sub-shell), being d^5/d^3 ions respectively. Therefore based on this principle, determining the number of near isotropic versus anisotropic ^{55}Mn tensors seen in the S_2 state should be able to differentiate between the HOS' and 'LOS' paradigms and define oxidation states of individual Mn centres, no Mn^{II} center should be present in this state [1]. But the ML signals observed have the 'spin projected' hyperfine interactions, due to the OEC being a sufficiently strongly exchanged coupled system (see below). Although the intrinsic 'single ion' hyperfine values are not seen, the fractional anisotropy of the hyperfine interactions will still be preserved, as the spin projection merely scales the overall tensor magnitude.

Illumination of spinach PSII membrane samples, which were dissolved in aqueous buffer medium with 3% ethanol (EtOH), is known to produce the most hyperfine structured broad form of the MLS [8]. Examples are shown in Figs. 1 and 2. The spectrum exhibits approximately 17 resolved peaks, with one resonance obscured by the tyrosine radical signal near $g = 2.00$ having been subtracted using the WINEPR software. This results in a gap within that region. This ML signal bears a resemblance to that from anti-ferromagnetically coupled Mn^{III}-Mn^{IV} or Mn^{III}-Mn^{II} oxo-briged dimers, though more lines are seen (signal ~180 mT wide) than typically seen in the model dimer compounds (16-peaks). In addition, a 'super-hyperfine' structure can be observed (~30 G spacing), especially in the upper field of the MLS [8]. The S_2 ML signal is narrower than that from a known model tetramer (Mn^{III}, $3Mn^{IV}$), which contains ~26 peaks and has a width of ~195 mT [9]. The strongly exchanged coupled centers of the OEC have net anti-ferromagnetic coupling in the S_2 state, with the ML signal arising from the $S_T = ½$ground state, where total spin operator, $S_T = S_1 + S_2 + S_3 + S_4$ (S_{1-4} are the spins of the four manganese ions). Therefore the observed individual nuclear hyperfine couplings are given as $\boldsymbol{A_i} = \rho_i$. $\boldsymbol{A_i(ion)}$, where ρ_i is the appropriate spin projection term for Mn centre i and these sum to unity for the total system. A typical sixteen line pattern of an anti-ferromagnetically coupled dimer (Mn^{III}-Mn^{IV}) forms, with the projection coefficients of $\rho_{III} = 2$ and $\rho_{IV} = -1$, ($\rho_{III} + \rho_{IV} = 1$). Here A_{III} is $\sim= 2 * A_{IV,}$ in isotropic value, while the Mn^{III}term is typically axial and highly anisotropic (Jahn-Teller d^4 ion), while Mn^{IV} is nearly isotropic (d^3 ion).

Jin et al (2014) have recently determined, from CW-EPR and electron nuclear double resonance (ENDOR) studies on the S_2 ML signal generated in PS II core complexes , as also used in the present study, that one large anisotropic Mn hyperfine coupling, one intermediate (near isotropic) coupling and one smaller, anisotropic coupling are clearly resolved for the ML signal. The two larger couplings are broadly consistent with a near 'isolated' Mn (III-IV) dimer scheme, while the smaller coupling approximately described the 'super-hyperfine' substructure seen within the main ML pattern lines. The presence of at least two strongly anisotropic couplings implies the presence of at least two Mn^{III} ions, i.e. the 'LOS' paradigm. The CW simulations performed by Jin et al. (2014) gave reasonable, semi-quantitative fits to the spectra, but were clearly somewhat deficient (too well defined substructure detail), particularly near the ML pattern edges. Since there were earlier indications from the NIR turnover experiments that the ML centre was probably not homogeneous, particularly with respect to factors affecting this fine substructure, it was decided to examine this issue further, using the 3% ethanol sample system that is known to produce the most structured forms of the broad ML species [8]. The possibility of a statistical spread of the smaller, anisotropic coupling values being present in samples as conventionally prepared was tested.

Using the excellent X-band CW-EPR S_2 multiline signals that were generated from high quality spinach PSII membranes preparations, with 3% EtOH in the buffer, as prepared in this project, the current proposal by Jin et al (2014) was tested to see if indeed Mn1 and Mn2 contribute the largest hyperfine values, with a variable anisotropic contribution from one other ion. A procedure of weighted computations was used, in an attempt to enhance the overall precision of simulations as well as to more realistically simulate peaks at the edges, the pattern and the line sub-structure observed, particularly in the up-field region of MLS signal

2 Materials and methods

2.1 PSII sample preparations

The PSII samples used in this project were obtained from fresh market spinach, commonly known as English Spinach (*Spinacia oleracea*). Market spinach was used as the source of plant material. The veins of these plant materials (spinach) were removed by tearing the vein away from the leaf (and weighing sets of about 100 grams), followed by washing the leaves in double distilled water to remove salt crusts which may have formed on the leaves and pesticides that may have been sprayed on the leaves. After washing these deveined leaves, they were then wrapped in paper towels wetted with distilled water and placed in the dark ready for PSII preparations. The protocol used in this project in isolating the PSII containing thylakoids membranes was by Bricker et al. [10] with modification by Smith et al. [11].

The homogenization, incubation steps as well as centrifugation were carried out in dim-green-light cold room, with temperature of about 4°C. The chlorophyll concentration determination was determined by using the method by Porra et al. [17]. Aliquots of 5-10 ml were placed in falcon tubes and stored at 8 to 15 mg/ml chlorophyll at -80 °C in the storage buffer (pH 6) consisting of 400 mM sucrose, 15 mM NaCl, 10 mM $MgCl_2$, 20 mM MES, 5 mM $CaCl_2$ for later use. For this experiment samples were prepared with 3% (v/v) ethanol (EtOH).

2.2 Illumination

The PSII samples (∼3% EtOH), prepared as described above, were thawed on ice/water mix (0 °C/273K) for 1 hour before use. Aliquots of 250 μl were carefully loaded into 4 mm O.D. quartz EPR tubes (Wilmad quartz), and subsequently frozen in liquid nitrogen. If bubbles were found in the sample, it was immediately thawed, the bubbles removed then re-frozen in liquid nitrogen (about 77 K). The annealing of PSII sample was done by storing the sample in ice/water mix (0 °C/273K) covered with a black cloth to minimise stray light entering. The sample was annealed for approximately 10 to 30 minutes, this ensured a full relaxation to the S_1 state, and subsequently freeze trapped in the S_1 state using liquid nitrogen. The S_1 state generates the background EPR spectrum, which is subtracted from an illumination spectrum to achieve the difference spectrum. The tyrosine radical (Y_D) signal was also removed from the difference spectrum. Otherwise the remaining tyrosine radical signal was subtracted using the Bruker WIN EPR system software package.

In order to generate the S_2 state signal, samples were subjected to continuous illumination at specific temperatures and wavelength ranges of light. To generate the S_2 state through $S_1 \rightarrow S_2$ turnover, from PSII membranes, the temperature of the sample was monitored and

controlled by a nitrogen gas flow system. Samples were subjected to 2 minutes illumination (temperature$\sim$ 200 K) using a Kodak Ektalite 1500 slide projector fitted with Halogen lamp (250 W). The light was passed through a 10 cm water path IR filter (to influence the S_1 to S_2 turnover, [12]), filtered using a combination of yellow and blue filters to allow a narrow window green light to pass. The sample was rapidly freeze trapped in the S_2 state immediately after illumination in liquid nitrogen (77 K).

2.3 EPR measurements

The experiments were performed using the X-band continuous wave (CW) Bruker Biospin ELEXSYS E500 spectrometer using Bruker SHQX resonant cavity and super X-EPR Microwave Bridge. The spectrometer was fitted with Oxford - ES900 continuous flow helium cryostat with temperatures controlled using Oxford Instruments ITC-4 temperature controller. The experiments were carried out at cryogenic temperatures ($\sim$ 6.5K). The EPR parameters used are listed in the figure legends; the magnetic field was calibrated with Bruker ER035M NMR Gaussmeter.

3 Results and discussions

Recently Jin et al. [2] reported ^{55}Mn hyperfine interactions above 400 MHz, ranging from $\sim$ 50 to $\sim$ 680 MHz as seen in the S_2 ML signal in plant PSII core complexes. The 'pure' broad ML form generated from the PSII membrane samples, in the presence of ethanol ($\sim$ 3% EtOH), used in this part of the present project, exhibited the highly structured ML spectra, similar to the that observed earlier by Jin et al. [2] in PSII core complex ML spectra (see Figs. 1, 2, 3, 4, 5, 6 and 7).

Figures 1a and b show the simulation of the experimental ML spectrum, using values close to the original hyperfine parameter set of Jin et al. (Table 1). As noted in the methods, this CW simulation is approximate, neglecting nuclear quadrupole terms (particularly on Mn1, where this is significant). However full matrix diagonalization was prohibitively expensive, computationally, for this four centre system. Although there is quite a reasonable match of the simulation to the data over much of the spectrum, near the edges the match is poorer, with too much 'regular' detail from the small hyperfine parameters (Mn3 particularly) present in the simulation. Examination of the simple splitting diagram shows that small variations in the two large couplings (Mn1 in particular) will vary the resultant hyperfine line positions mostly at the edges (where the nuclear m_I values are $\pm$ 5/2). Thus a (small) variation-spread in the Mn1 and Mn2 parameter magnitudes will 'blur' (through overlapping interference) fine features (from Mn3 and 4) most at the ML pattern edges. This is the basis of the approach taken here. Obviously there is a lot of potential 'freedom' in choosing such a parameter spread, which still must be relatively small otherwise all fine detail in the ML pattern would be lost. Several possibilities were examined and the two most promising are indicated here

The weighted computation method used depends on varying both the precise hyperfine values and their statistical weights (fractional contributions to the total spectrum). The mean values about which this spread occurs are taken essentially as those determined earlier by Jin et al. (i.e. Table 1 values). Only variations in the Mn1 and 2 hyperfine parameters were considered, with variation magnitudes of order $\sim$5 MHz (see supplementary material).

The simulations of the X-band CW-EPR generated S_2 multiline signals were performed in Easyspin function 'pepper' [13], using the 2nd perturbation option (4 manganese ions).

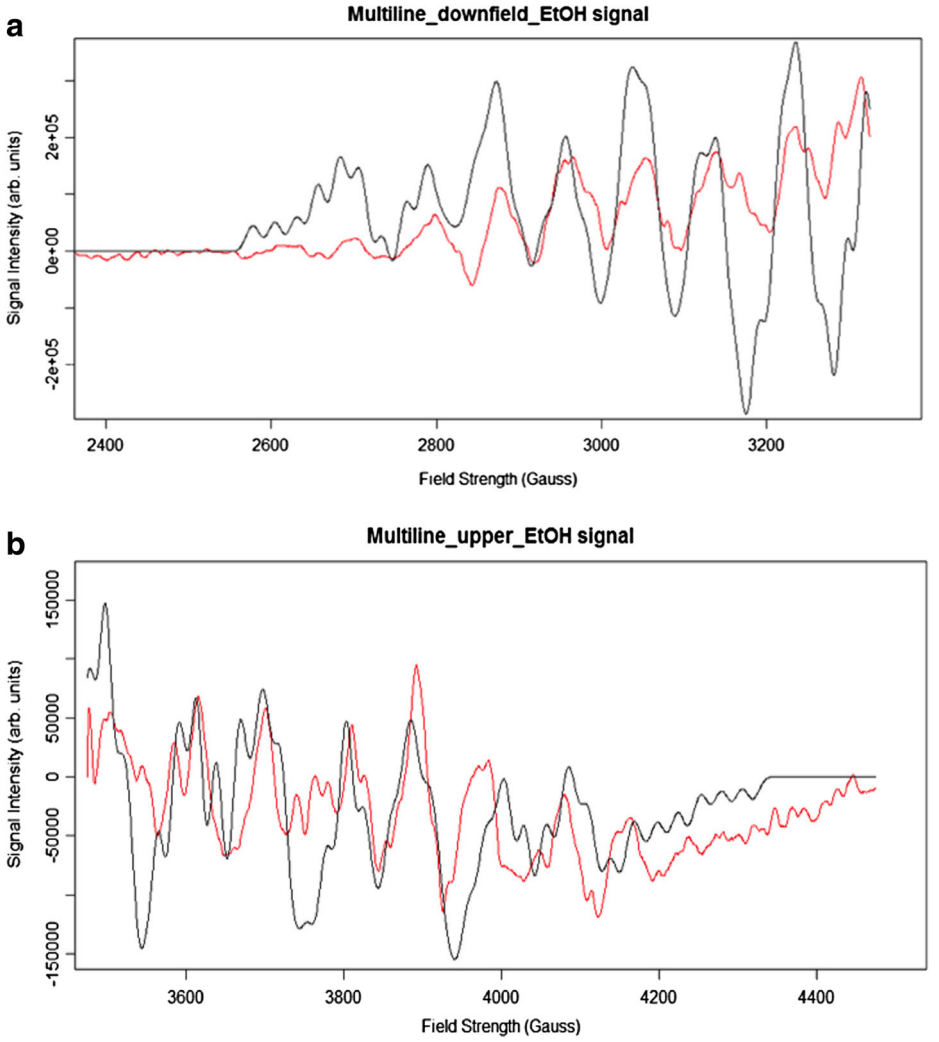

Fig. 1 **a** The X-band CW-EPR difference down- field ML region. Experimental spectrum (red) and best-fit simulation (black). Spectrometer conditions: centre field 282.5 mT; frequency 9.634273 GHz; modulation amplitude 9.6 Gauss; microwave power 0.5 mW; sweep width 100 mT; number of points 2500; spectrum is average of 30 scans, temperature 6.5 K (see supplementary material *S1* of this paper for parameters used for simulation). **b** The X-band CW-EPR difference up- field ML region. Experimental spectrum (red) and best-fit simulation (black). Spectrometer conditions: centre field 397.5 mT; frequency 9.634261 GHz; modulation amplitude 9.6 Gauss; microwave power 0.5 mW; sweep width 100 mT; number of points 2500; spectrum is average of 30 scans; temperature 6.5 K (see supplementary material *S2* of this paper for parameters used for simulation)

As noted the nuclear quadrupole interactions were not included. The initial estimates of the hyperfine tensors and g tensors were obtained from Jin et al. [2] with some adjustments in the Mn1 and Mn2 hyperfine values, line-width 1.6 mT as well as Mn3 Euler angles (α and γ). The simulated spectra are shown in Figs. 2–7, and the central parameters used are listed in Table 1 below. The computer simulation of the ML signal yielded the black spectra

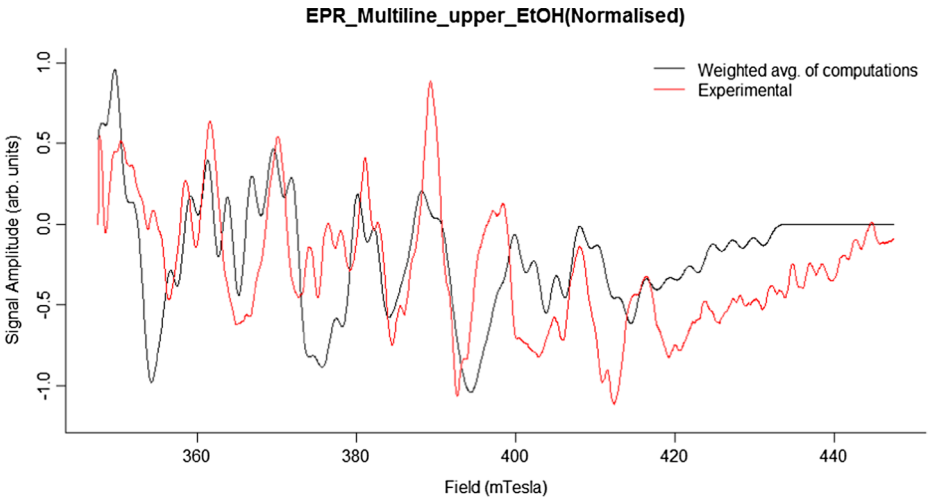

Fig. 2 The X-band CW-EPR difference up- field ML region. Experimental spectrum (red) and best-fit simulation (black), which was the average of 3 weighted computations. Spectrometer conditions: centre field 397.5 mT; frequency 9.634261 GHz; modulation amplitude 9.6 Gauss; microwave power 0.5 mW; sweep width 100 mT; number of points 2500; spectrum is average of 30 scans; temperature 6.5 K. The parameters used for simulations are listed in Table 1, as well as weighted average of computations method in supplementary material *S3* of this paper

(after averaging three weighted computations, see Figs. 2, 3 and 4, and seven weighted computations, see Figs. 5, 6 and 7), The experimental spectra are represented in red in these figures.

As concluded by Jin et al., the A_{IV} term from Mn2 is reasonably isotropic and determines the $\sim$ 90 Gauss main line pattern spacing in anti-ferromagnetically coupled Mn^{III}-Mn^{IV} dimers [14, 15]. The ML region near g= 2 exhibits some deviation from the simulated values, as seen earlier by Jin et al. [2], which reflects imperfect subtraction of the strong background features (mainly Y_D) in the difference spectrum. Figures 3 and 6 represent the expanded downfield (below g=2) region of the 'pure broad' multiline wide spectrum generated, with less evidence of pattern splitting compared to the up- field (above g=2) region of the spectrum, in Figs. 2 and 5. This means, as Jin et al. [2] suggested, that it likely arises not from an intrinsic line-width effect, but from an anisotropic hyperfine interaction. This is further supported by the fact that the splitting is not uniform on each main line of the pattern, but seen approximately on every second resonance in the upper field region, with a coupling of $\sim$30 Gauss. Most likely this arises from Mn3 which like Mn1 is highly anisotropic in symmetry, although the overall magnitude of its contribution is small. Hence one centre should have a small ρ value as Jin et al. [2] earlier suggested ($\sim$ 0.2, which is consistent with Mn3 from Table 1, where 45/226 $\sim$ 0.2), that the OEC cluster should have two centres with small ρ –values, was also predicted by density matrix renormalisation group theory, which is the highest -level quantum chemical calculation yet performed on the OEC [16]. These calculations also predicted one large ρ value ($\sim$2) and one intermediate coupling (ρ $\sim$-1), even though a high oxidation state assumption was used for the OEC. The large coupling was for the single Mn III centre, which was Mn1 in the study of Kurashige et al. [16].

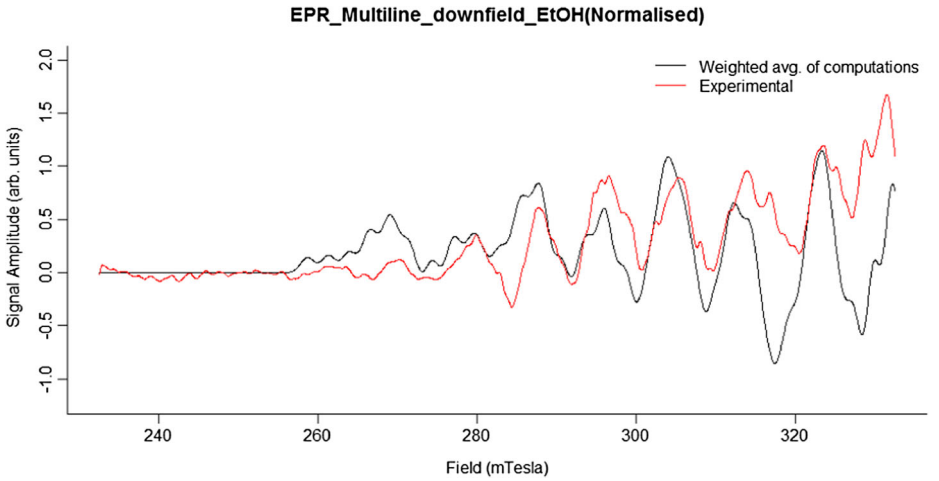

Fig. 3 The X-band CW-EPR difference down- field ML region. Experimental spectrum (red) and best-fit simulation (black), which was the average of 3 weighted computations. Spectrometer conditions: centre field 282.5 mT; frequency 9.634273 GHz; modulation amplitude 9.6 Gauss; microwave power 0.5 mW; sweep width 100 mT; number of points 2500; spectrum is average of 30 scans, temperature 6.5 K. The parameters used for simulations are listed in Table 1, as well as weighted average of computations method in supplementary material*S4* of this paper

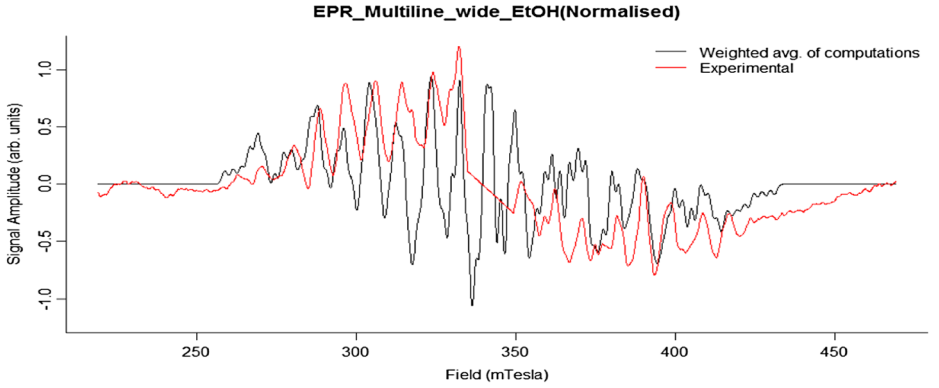

Fig. 4 The X-band CW-EPR difference multiline wide experimental spectrum (red) and best-fit simulation (black), which was the average of 3 weighted computations. Spectrometer conditions: centre field 344 mT; frequency 9.634187 GHz; modulation amplitude 9.6 Gauss; microwave power 1 mW; sweep width 250 mT; number of points 2500; spectrum is average of 30 scans; temperature 6.5 K. The parameters used for simulations are listed in Table 1, as well as weighted average of computations method in supplementary material *S5* of this paper

The parameters used here in simulating the ML signal, as indicated in Table 1, also show large nuclear hyperfine values for Mn1 and Mn2, consistent with ρ values of $\sim$ 2 and -1 respectively, while nuclear hyperfine values for Mn3 and Mn4 are less than 100 MHz, consistent with the results of Jin et al. [2]. Quadrupole interactions were not included in

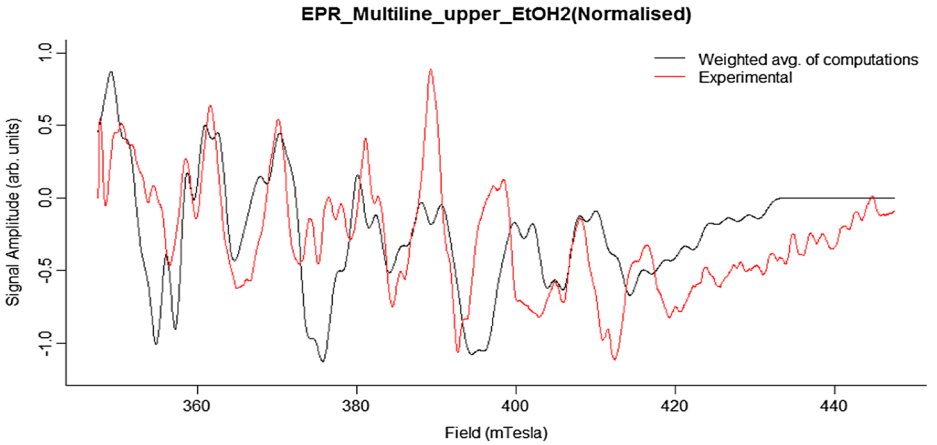

Fig. 5 The X-band CW-EPR difference up- field ML region. Experimental spectrum (red) and best-fit simulation (black), which was the average of 7 weighted computations. Spectrometer conditions: centre field 397.5 mT; frequency 9.634261 GHz; modulation amplitude 9.6 Gauss; microwave power 0.5 mW; sweep width 100 mT; number of points 2500; spectrum is average of 30 scans; temperature 6.5 K. The parameters used for simulations are listed in Table 1, as well as weighted average of computations method in supplementary material *S6* of this paper

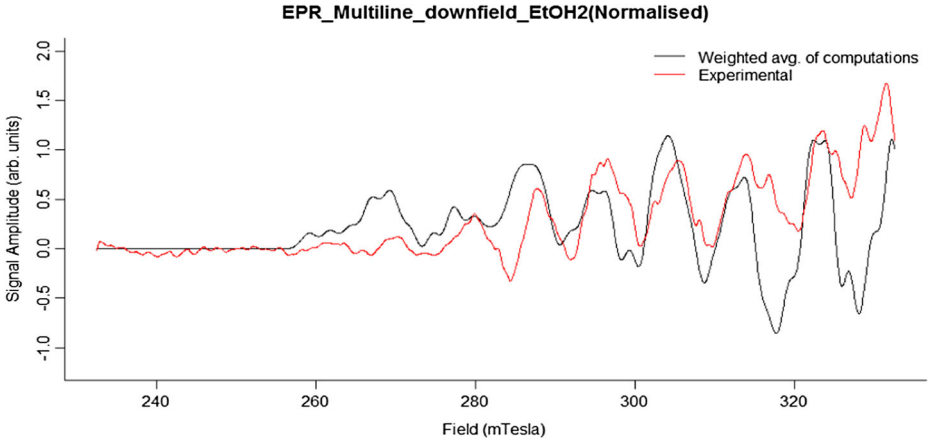

Fig. 6 The X-band CW-EPR difference down- field ML region. Experimental spectrum (red) and best-fit simulation (black), which was the average of 7 weighted computations. Spectrometer conditions: centre field 282.5 mT; frequency 9.634273 GHz; modulation amplitude 9.6 Gauss; microwave power 0.5 mW; sweep width 100 mT; number of points 2500; spectrum is average of 30 scans; temperature 6.5 K. The parameters used for simulations are listed in Table 1, as well as weighted average of computations method in supplementary material *S7* of this paper

these simulations, but the nuclear hyperfine values for Mn4 are very small and from Table 1, the hyperfine values for Mn1 and Mn3 are highly anisotropic and almost rhombic, which means they must have Mn^{III} oxidation states, as Jin et al. [2] proposed. Mn2 hyperfine values are the least anisotropic, so the likely oxidation state of this ion is Mn^{IV}. The fitted

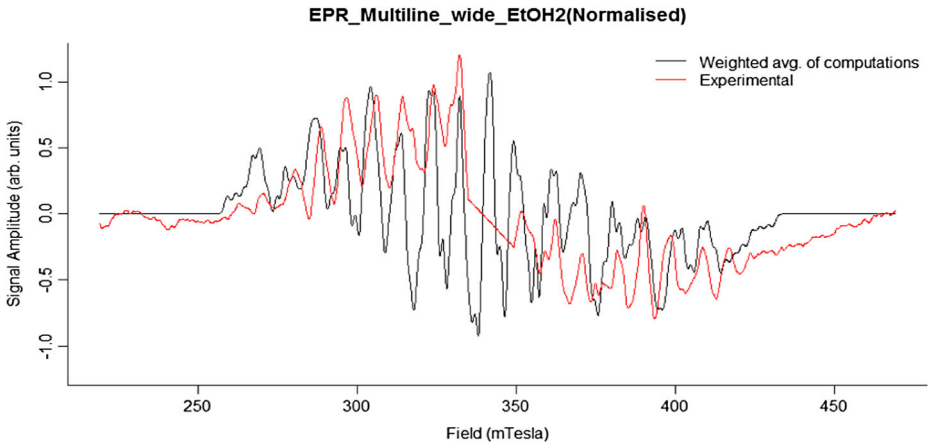

Fig. 7 The X-band CW-EPR difference multiline wide experimental spectrum (red) and best-fit simulation (black), which was the average of 7 weighted computations. Spectrometer conditions: centre field 344 mT; frequency 9.634187 GHz; modulation amplitude 9.6 Gauss; microwave power 1 mW; sweep width 250 mT; number of points 2500; spectrum is average of 30 scans; temperature 6.5 K. The parameters used for simulations are listed in Table 1, as well as weighted average of computations method in supplementary material *S8* of this paper

parameters for Mn4 are very small but also highly anisotropic, hence this ion is likely to be Mn^{III}.

The isotropic values (A_{iso}) of Mn1 and Mn2 are -487 and 226 respectively, which is consistent with the above suggested spin projection values. The maximum hyperfine coupling for Mn1 is ∼600 MHz (A_{Mnx}), with a total anisotropic range of ∼280 MHz. The Mn1 hyperfine tensor has a high degree of anisotropy (280/487*100) ∼57%, making it near rhombic (matching the conclusion of Jin et al. [2]). Mn2 has a maximum hyperfine tensor coupling of ∼276 MHz, with a total anisotropic range of 111, giving a fractional anisotropy of (111/226*100) ∼49%, which is substantial anisotropy for a Mn^{IV} centre. Mn3 has maximum hyperfine tensor coupling of ∼78 MHz, and A_{iso} of ∼ 45, with a hyperfine tensor which is completely anisotropic (rhombic). Again Mn4 has A_{iso} of ∼ 7 and is also totally rhombic in symmetry. Therefore based on this simulation, the likely oxidation paradigm of the manganese cluster is Mn^{III} Mn^{IV} Mn^{III} Mn^{III}, the 'LOS' paradigm. The large magnetic exchange coupling contributions come from Mn1 and Mn2, while Mn3 and Mn4 contributions are small <100 MHz. This is totally consistent with the 'dimer of dimers'.

Lastly, the results in Figs. 2–7 support the idea that some statistical spread in Mn hyperfine parameter values, particularly for Mn1 and Mn2, are present in the S_2 state as conventionally prepared, even the highly resolved broad form examined here. The cosmetic fits, particularly near the pattern edges are improved with this assumption, although it is clear that the precise nature of this parameter spread is yet to be fully understood. Interestingly the three component weighted average spectra in Figs.2-4 is probably a better fit to the data than the seven component weighted average spectra, suggesting that perhaps only a small number of near-equivalent-ML forms are co-generated in the experimental spectra. Presumably only some of these are then responsive to NIR induced turnover to the g4.1 state of S_2.

Table 1 Showing fitted simulation (2^{nd} order perturbation theory) parameters to the X-band CW-EPR S_2 ML signal (broad, down-field and upper field) of the PSII membrane plus ∼3% EtOH samples

Parameter	*x*	*y*	*z*	*Isotropic value*
g	1.989	2.008	1.964	1.987
A_{Mn1}	−600	−542	−320	−487
A_{Mn2}	165	237	276	226
A_{Mn3}	−78	−12	−46	−45
A_{Mn4}	1	20	1	7
Euler angles	α	β	γ	–
Mn1	0	0	0	–
Mn2	0.422	0.750	−0.737	–
Mn3	−0.136	0.210	0.378	–
Mn4	0	0	0	–
Linewidth	16 Gauss			

The isotropic values were calculated from $A_{Mni,iso} = (A_{Mnix} + A_{Mniy} + A_{Mniz})/3$, where i =1-4, and $g_{iso} = (g_x + g_y + g_z)/3$. Units for A-values are in MHz, Euler angles in radians, v ∼9.634187 GHz, line-width 1.6 mT. (NB. The hyperfine values indicated were taken as 'the central mean' in performing the weighted computations method)

4 Conclusions

The ML signal simulation, favour the oxidation pattern of the manganese cluster to be Mn^{III} Mn^{IV} Mn^{III} Mn^{III}, which is referred to as the 'LOS' paradigm in the S_2 state. The simulations of the X-band CW-EPR multiline spectra, revealed the presence of three manganese ions having hyperfine couplings with large anisotropy, which makes them likely to be Mn^{III}. This clearly support the 'LOS' paradigm model, with the mean oxidation level of 3.25 in the S_2 state. The magnetic exchange coupling is totally consistent with the 'dimer of dimers'.This agrees with the earlier data of Jin et al. [2]. However, the simulations suggest that there is likely a degree of heterogeneity in the Mn hyperfine couplings, probably of Mn1 and Mn2, in the S_2 ML state as conventionally prepared. Terrett et al. recently computed isolated ion ^{55}Mn hyperfine tensors from ABAB and ABBA configurations for the 'open' form structures, using two different functionals with relativistic corrections. Their calculations show that, cluster internal interactions is magnetically close to a 'coupled dimers' configuration, and this is plausible in the 'LOS' paradigm for an 'open' form of the cluster geometry [7].

Acknowledgments The author gratefully acknowledge financial support from the Australian Research Council. Bernard Baituti also acknowledges the generous scholarships provided by the Botswana International University of Science and Technology (BIUST) and ANU.

Author Contributions Dr Bernard Baituti-prepared the PSII samples and performed EPR measurements, performed the simulations, prepared the manuscript.

References

1. Gatt, P., Stranger, R., Pace, R.: Application of computational chemistry to understanding the structure and mechanism of the Mn catalytic site in photosystem II–a review. J. Photochem. Photobiol. B **104**(1–2), 80–93 (2011). Available at, http://www.ncbi.nlm.nih.gov/pubmed/21396828
2. Jin, L., et al.: Electronic structure of the oxygen evolving complex in photosystem II, as revealed by (55)Mn Davies ENDOR studies at 2.5 K. Phys. Chem. Chem. Phys. (PCCP) **16**(17), 7799–812 (2014). Available at, http://www.ncbi.nlm.nih.gov/pubmed/24643307
3. Dismukes, G.C., Siderer, Y.: Intermediates of a polynuclear manganese center involved in photosynthetic oxidation of water. Proc. Natl. Acad. Sci. U. S. A. **78**(1), 274–278 (1981)
4. Gatt, P., Petrie, S., Stranger, R., Pace, R.J.: Rationalizing the 1.9 Å crystal structure of photosystem II-A remarkable Jahn-Teller balancing act induced by a single proton transfer. Angew. Chem. Int. Ed. **51**, 12025–12028 (2012)
5. Petrie, S., Stranger, R., Pace, R.: J. Rationalising the geometric variation between the a and b monomers in the 1.9 Å crystal structure of photosystem II. Chem. A Eur. J. **21**, 6780–6792 (2015)
6. Terrett, R., Petrie, S., Pace, R.J., Stranger, R.: What does the Sr-substituted 2.1 Å resolution crystal structure of photosystem II reveal about the water oxidation mechanism . Chem. Commun. (Camb). **50**, 8–11 (2014). https://doi.org/10.1039/c3cc49324e
7. Terrett, R., Petrie, S., Stranger, R., Pace, R.J.: What computational chemistry and magnetic resonance reveal concerning the oxygen evolving centre in Photosystem II. J. Inorg. Biochem. https://doi.org/10.1016/j.jinorgbio.2016.04.009 (2016)
8. Ahrling, K., Pace, R., Evans, M.: The Catalytic Manganese Cluster:Implications from Spectroscopy. In: Wydrzynski, T.J., Satoh, K. (eds.) Photosystem II The Light Driven Water:Plastoquinone Oxidoreductase, pp. 285–305. Springer, The Netherlands (2005)
9. Blondin, G., et al.: Electron paramagnetic resonance study of the S=1/2 ground state of a radiolysis-generated manganese(III)-trimanganese(IV) form of [Mn-IV;O-4(6)(bipy)(6)](4+) (bipy=2,2'-bipyridine). Comparison with the photosynthetic Oxygen Evolving Complex, vol. 28 (1997)
10. Bricker, T.M., Pakrasi, H.B., Sherman, L.A.: Characterization of a spinach photosystem II core preparation isolated by a simplified method. Arch. Biochem. Biophys. **237**(1), 170–176 (1985)
11. Smith, P.J., Ahrling, K.A., Pace, R.J.: Nature of the S2 state electron paramagnetic resonance signals from the oxygen-evolving complex of photosystem II: Q-band and oriented X-band studies. J. Chem. Soc. Faraday Trans. **89**, 2863–2868 (1993)
12. Smith, P.J., Masters, V.M., Peterson, S., Wydrzynski, T., Styring, S., Pace, R.J., Krausz, E.: Magneto-optical measurements of the pigments in fully active photosystem II core complexes from plants. Biochemistry **41**, 1981–1989 (2002)
13. Stoll, S., Schweiger, A.: EasySpin, a comprehensive software package for spectral simulation and analysis in EPR. J. Magn. Reson. **178**(1), 42–55 (2006)
14. Teutloff, C., et al.: High-field EPR investigations of MnIIIMnIV and MnIIMnIII states of dimanganese catalase and related model systems. Magn. Reson. Chem., 43(PEC. ISS.) (2005)
15. Schäfer, K.O., et al.: Multifrequency EPR investigation of dimanganese catalase and related Mn(III)Mn(IV) complexes. J. Phys. Chem. B **107**(5), 1242–1250 (2003)
16. Kurashige, Y., Chan, G.K.-L., Yanai, T.: Entangled quantum electronic wavefunctions of the Mn4CaO5 cluster in photosystem II. Nat. Chem. **5**(8), 660–6 (2013). https://doi.org/10.1038/nchem.1677
17. Porra, R.J., Thompson, W.A., Kriedemann, P.E.: 320.pdf. Biochimica et Biophysica Acta **975**, 384–394 (1989)
18. Satoh, K., Wyrdzynski, T.J., Govindjee: Introduction to photosystem II, in Photosystem II: The Light-Driven Water. Plastoquinone Oxidoreductase **22**, 11–22 (2005)
19. Koulougliotis, D., Hirsh, D.J., Brudvig, G.W.: JACS **114**, 8322–8323 (1992)
20. Pace, R.J., Stranger, R., Petrie, S.: Why nature chose Mn for the water oxidase in Photosystem II. Dalt. Trans. **41**(24), 7179 (2012)
21. Umena, Y., Kawakami, K., Shen, J.-R., Kamiya, N.: Crystal structure of oxygen-evolving photosystem II at a resolution of 1.9 Å. Nature **473**, 55–60 (2011)
22. Koua, F.H.M., Umena, Y., Kawakami, K., Shen, J.-R.: Structure of Sr-substituted photosystem II at 2.1 A resolution and its implications in the mechanism of water oxidation. Proc. Natl. Acad Sci **110**, 3889–3894 (2013)
23. Suga, M., Akita, F., Hirata, K., Ueno, G., Murakami, H., Nakajima, Y., Shimizu, T., Yamashita, K., Yamamoto, M., Ago, H., Shen, J.-R.: Nature (2014)

24. Jaszewski, A.R., Petrie, S., Pace, R.J., Stranger, R.: Toward the assignment of the manganese oxidation pattern in the water-oxidizing complex of photosystem II: A time-dependent DFT study of XANES energies. Chem. Eur. J. **17**(20), 5699–5713 (2011)
25. Yachandra, V.K., Sauer, K., Klein, M.P.: Manganese cluster in photosynthesis: Where plants oxidize water to dioxygen. Chem. Rev. **96**, 2927–2950 (1996)
26. a Pantazis, D., Ames, W., Cox, N., Lubitz, W., Neese, F.: Two interconvertible structures that explain the spectroscopic properties of the oxygen-evolving complex of photosystem II in the S2 state. Angew. Chem. Int. Ed. Engl. **51**(39), 9935–40 (2012)
27. Campbell, K.A., et al.: The 23 and 17 kDa extrinsic proteins of Photosystem II modulate the magnetic properties of the S1-state manganese cluster. Biochemistry **37**, 5039–5045 (1998)
28. Kok, B., Forbush, B., McGloin, M.: Cooperation of charges in photosynthetic O2 evolution-1. A linear four step mechanism. Photochem. Photobiol. **11**, 457 (1970)
29. Liang, W., Roelofs, T.A., Cinco, R.M., Rompel, A., Latimer, M.J., Yu, M.O., Sauer, K., Klein, M.P., Yachandra, Y.K.: Structural change of the Mn cluster during the S-2 –> S-3 state transition of the oxygen-evolving complex of photosystem II. Does it reflect the onset of water/substrate oxidation? Determination by Mn X-ray absorption spectroscopy. JACS **122**, 3399–3412 (2000)
30. Robblee, J.H., Messinger, J., Cinco, R.M., et al.: The Mn Cluster in the S_0 State of the Oxygen-Evolving Complex of Photosystem II Studied by EXAFS Spectroscopy: Are There Three Di-μ-oxo-bridged Mn_2 Moieties in the Tetranuclear Mn Complex. J. American Chem. Soc. **124**(25), 7459–7471 (2002)
31. Glöckner, C., Kern, J., Broser, M., Zouni, A., Yachandra, V., Yano, J.: Structural changes of the oxygen-evolving complex in photosystem II during the catalytic cycle. J. Biol. Chem. **288**(31), 22607–22620 (2013)
32. Haumann, M., et al.: Structural and oxidation state changes of the photosystem II manganese complex in four transitions of the water oxidation cycle (S0 –> S1, S1 –> S2, S2 –> S3, and S3,4 –> S0) characterized by X-ray absorption spectroscopy at 20 K and room temperature. Biochemistry **44**, 1894–1908 (2005)
33. Yano, J., Yachandra, V.: Mn4Ca cluster in photosynthesis: Where and how water is oxidized to dioxygen. Chem. Rev. **114**, 4175–4205 (2014)
34. Seigbahn, P.E.M.: Mechanisms for proton release during water oxidation in the S2 to S3 and S3 to S4 transitions in photosystem II. Phys. Chem. Chem. Phys **14**, 4849–4856 (2012)
35. Saito, T., et al.: Possible mechanisms of water splitting reaction based on proton and electron release pathways revealed for CaMn4O5 cluster of PSII refined to 1.9? X-ray resolution. Int. J. Quantum Chem. **112**(1), 253–276 (2012)
36. Yamanaka, S., et al.: Structure and reactivity of the mixed-valence CaMn4O 5(H2O)4 and CaMn4O 4(OH)(H2O)4 clusters at oxygen evolution complex of photosystem II. Hybrid DFT (UB3LYP and UBHandHLYP) calculations. Int. J. Quantum Chem. **112**(1), 321–343 (2012)
37. Kusunoki, M.: S1-state Mn4Ca complex of Photosystem II exists in equilibrium between the two most-stable isomeric substates: XRD and EXAFS evidence. J. Photochem. Photobiol. B Biol. **104**, 100–110 (2011)
38. Krewald, V., et al.: Metal oxidation states in biological water splitting. Chem. Sci. **6**(3), 1676–1695 (2015)
39. Yano, J., et al.: X-ray damage to the Mn4Ca complex in single crystals of photosystem II: A case study for metalloprotein crystallography. Proc. Natl. Acad. Sci **102**, 12047–12052 (2005)
40. Liang, W., et al.: Correlation between structure and magnetic spin state of the manganese cluster in the oxygen-evolving complex of photosystem II in the S2 state: Determination by X-ray absorption spectroscopy. Biochemistry **33**, 4923–4932 (1994)
41. Peloquin, J.M., Campbell, K.A., Randall, D.W., Evanchik, M.A., Pecoraro, V.L., Amstrong, W.H., Britt, R.D.: ^{55}Mn ENDOR of the S2-state multiline EPR signal of photosystem II: Implications on the structure of the tetranuclear Mn cluster. JACS **122**, 10926 (2000)